Optical Measurements of Two Cylindrical and Conical Heavy-Duty Diesel Injector Nozzels – A Comparison of Reference Diesel, HVO, and RME Fuels

Hamidreza Fajri[a,*], Sebastian Rieß[a], Rafael Clemente Mallada[a], Ilona Ruoff[b], Michael Wensing[a]

[a]Professorship for Fluid Systems Technology, FAU Erlangen-Nürnberg, Germany
[b]Woodward L'Orange GmbH, Stuttgart, Germany

*Corresponding author. Tel: +49-911-3731705
Fax: +49-911-3731360
E-mail address: Hamidreza.fajri@fau.de (H. Fajri)

Abstract:

In the present work, a constant volume/constant pressure combustion chamber was utilized to measure the major parameters of vapour/liquid phases and combustion of fuel spray introduced by two heavy-duty, large-diameter diesel injectors. A conical nozzle (K factor 4) with a 300 µm outlet diameter and a 1300 µm length and a cylindrical nozzle (K factor 0) with a 300 µm outlet diameter and a 650 µm length display notably distinct impacts on the formation of the mixture, the air entrainment process, and the combustion behaviour. Several parameters, including jet and liquid spray penetration lengths, jet cone angle, and jet projected area are combined to describe spray characteristics in an inert background gas, and ignition incidence, flame lift-off length, and soot appearance time parameters are calculated to explain the combustion trend of the nozzles in a reactive gas background. These observations were conducted using four distinct optical techniques, two of Schlieren and Mie-Scattering for inert condition, and two of OH* Chemiluminescence and Natural Flame Luminosity for reactive condition. This study collects a wide variety of boundary conditions, comprising ambient pressure/temperature and fuel rail pressure, with diverse fuels, including reference diesel, HVO, and RME fuels.

The findings are categorized by the jet and liquid spray behaviours in the first part, demonstrating that the jet cone angle is an injector geometry-based parameter and that the cylindrical nozzle has a larger cone angle and a shorter liquid spray length. Three distinct scenarios of the computed air-to-fuel mass ratio at the same axial positions, time steps, and injected fuel mass indicate a marginally higher air entrainment in the cylindrical nozzle and, presumably, a faster and better mixture formation. The thorough examination of the combustion characteristics indicates that a quicker formation of the initial stoichiometric region in the cylindrical nozzle results in a shorter ignition delay at most experimental locations, which ultimately results in a faster soot initiation. However, depending on the flame lift-off length and the boundary conditions, the interval between ignition and the development of soot varies considerably. Finally, it is demonstrated that, with the exception of fuel pressure variation, the flame lift-off length, which is crucial in providing the initial mixture formation prior to combustion occurrence, follows the ignition delay trend and exhibits a shorter length with a shorter ignition delay.

Keywords:

Bio-diesel Fuels; Schlieren; Mie-Scattering; OH* Chemiluminescence; Natural Flame Luminosity; Heavy-duty Injector

Introduction:

Spray propagation, air/fuel mixture formation, combustion initiation and development, and exhaust gas emissions are significantly impacted by the geometry of diesel injectors [1-4]. In recent years, research has been conducted on cavitation phenomena, jet and liquid spray parameters, and fuel combustion in constant volume chambers (CVCs) and optical engines to illustrate how nozzle geometries influence mixture formation and

emission production [5-13]. The fundamental governing phenomena on the spray and combustion parameters have been identified and synchronized in these studies using a variety of optical and laser diagnostics, including optical Schlieren, Mie-Scattering, OH* Chemiluminescence, and Natural Flame Luminosity, as well as laser methods such as Raman Spectroscopy and Laser-Induced Fluorescence (LIF) measurements [2, 8, 14-18]. These approaches along with different fuels and injectors have been employed to develop empirical 1D models to predict jet penetration, air entrainment, flame lift-off length (FLoL), and the relationship between ignition delay and ambient parameters. These equations, which have been validated with experimental data, have aided in describing spray and combustion parameters, in particular by providing an overview of the effective parameters on air entrainment [19-23]. In addition to diesel nozzle geometries, the effects of alternative bio-diesel fuels such as Rapeseed Oil Methyl Esters (RME) and Hydrotreated Vegetable Oil (HVO), the first and second bio-diesel generations, respectively, as a pure and/or additive on combustion and pollution formation were studied in CVCs, optical and real engines [24-27].

Cavitation formation, near-nozzle turbulence intensity, pressure distribution, mass flow rate, and fuel droplet atomization are all significantly influenced by nozzle geometry characteristics [5]. These relationships indicate that higher cavitation formation itself has the potential to affect the fuel mass flow rate in cylindrical nozzles at high injection pressure, whereas lower cavitation increases the discharge coefficient in conical nozzles [6]. Researchers also established a proportional relationship between the momentum flux and the nozzle pressure drop, as well as a gradual acceleration of flow and a slight change in flow direction in conical nozzles [7].

Cavitation has the capability to cause major disturbance in the surrounding environment and amplifies the oscillations in the spray cone angle. However, it also has certain beneficial impacts on mixture formation. By forming the cavitation, cylindrical nozzles may very well be able to improve injection velocity and increase cone angle, while reducing effective diameter. On the other hand, the cavitation tends to boost spray mixing and momentum exchange, resulting in more turbulent velocity profiles at the nozzle exit, ultimately leading to better mixture formation [8, 10, 28].

In light-duty injectors, the correlation between nozzle geometries and ignition, flame development, and FLOL has also been examined [11-13]. Payri et al. [11] studied two different nozzles with varying K factors and entrance diameters and came to the conclusion that conicity can accelerate ignition initiation. It was shown that various combustion processes are significantly influenced by the size and configuration of nozzles. In contrast, Som et al. [13] found that conicity has the reverse effect, causing ignition to occur further downstream from the spray; the employed nozzles had equal entry diameters but differing K values. In accordance with the literatures, the appearance of ignition and FLoL may vary based on the rate at which the nozzle forms the initial mixture, which is controlled by its geometry, mass flow rate, K factor, and exit diameter. This is the main justification for keeping track of the various study results.

Understanding how mixture formation and flame propagation affect emission production, particularly the formation of nitrogen oxide and soot, is unquestionably the ultimate goal of research into spray and combustion. Thereupon, Farajollahi et al. [3] used CFD simulations to compare conical and cylindrical nozzles on a heavy-duty engine, finding that the convergent conical nozzle significantly reduces nitrogen oxide emissions due to a more uniform temperature distribution. Contrarily, higher nozzle cavitation rates result in smaller spray droplets, better mixing, and more nitrogen oxide while producing less soot due to a reduced equivalence air-to-fuel ratio at FLoL [4, 29]. The researchers managed to demonstrate that a cylindrical nozzle can reduce soot formation due to its cavitation formation, but it is not a good solution for nitrogen oxide reduction.

The bio-diesel fuels (RME and HVO) have been intriguing to compare with diesel fuel since both are typically capable of lowering emission production under real-world engine conditions, although some earlier research came to conflicting conclusions and claimed they were not a good solution, see [24, 27, 30, 31] and references therein. The promises for CO2 reduction varied from study to study as well, and authors reported varying results for CO2 emissions reduction at the tailpipe [25, 26, 32]. Although using bio-diesel fuels may reduce emissions, it seems important to assume that real engine design and calibration procedures are the most relevant aspects for achieving a range of bio-diesel fuel assessment results.

In recent years, some studies have made efforts to address heavy-duty injectors. Payri et al. [33] used the basic spray optical methods including Mie-scattering and Schlieren methods, and have resulted a proportional effect of heavy-duty nozzle diameter on vapour penetration. Balz et al. [34, 35] with a two-stroke marine diesel engines have looked into the combustion and in-nozzle flow using a variety of optical methods, such as diffuse back-illumination, flame luminosity, and OH* Chemiluminescence, and came to the conclusion that in-nozzle flow cavitation patterns play a significant role for the eccentric nozzle design, which generates an asymmetrical spray contour and has a significant influence on the injection mass and velocity profile. As a comparison between light-duty and heavy-duty injectors with the same optical methods, Payri et al. [36] discovered that increasing orifice diameter increases lift-off length, speeds up the rate of flame penetration, promotes soot formation, and changes the combustion model from one with no liquid-flame interaction to one with a more complex liquid-vapour and flame interaction. Moreover, some laser methods such as OH-PLIF and PAH-PLIF have been targeted to examine the mixture development and emission formation, and explored that a narrow-angle injection results in reduced soot formation and improved late-cycle oxidation of fuel-lean regions at the center of the combustion chamber [37]. Despite the fact that the optical and laser diagnostics used in heavy-duty studies are comparable with light-duty injectors, there has been a severe lack of research on large-nozzle injectors specifically to compare the effect of nozzle geometry on spray and combustion developments.

The current study examines the effects of nozzle shapes on the main spray parameters, ignition, and soot initiations using a combination of heavy-duty nozzles, bio-diesel, and diesel fuels. This is a follow-up to the authors' earlier study [16], which evaluated how specific spray parameters were impacted by thermodynamic conditions. However, the current study main objective is to determine nozzle geometry effects on the vapour and liquid phases of spray, as well as the ignition delay and combustion behaviour.

Experimental Facilities:

A constant volume and constant pressure combustion chamber accessible at the Fluid System Technology (FST) Institute at FAU Erlangen-Nürnberg makes it feasible to scavenge 10 liters of chamber volume with a freely adjustable composition of air and nitrogen or pure air/pure nitrogen and adjust various thermodynamic conditions by adjusting up to the maximum allowable pressure and temperature, which are 10 MPa and 1000 K, respectively. The windows size of 75 mm from nozzle tip is available to detect the spray and combustion regions. To obtain more information about the chamber, see [38] and references therein. Figure 1 depicts the FST CVC chamber and shows the positions of the fuel cooling fluid and entrance heaters as well as where gas enters and exits the chamber.

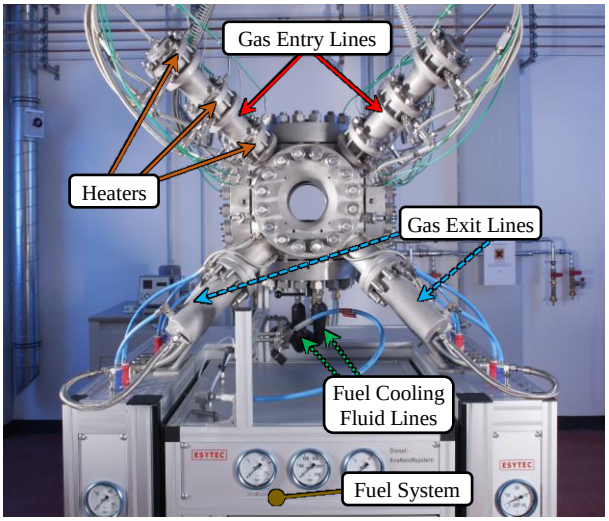

Figure 1. Constant Volume/Constant Pressure Chamber

Optical methods and Spray Evaluation

This study focus on the jet and liquid spray phases in an inert background condition and the combustion characteristics in a reactive background condition. Therefore, to visualize and quantify the jet and liquid spray phases, Mie-Scattering and Schlieren photography were used in the first section.

Schlieren:

The Schlieren method operates by delivering parallelized light beams (produced by a simple LED array - Hardsoft IL-106 Green) across the chamber via two collimator lenses. Variations in the densities of fuel and air, as well as the reflection of light beams, result in optical inhomogeneity inside the chamber, which are finally captured by a high-speed PHOTRON SA-Z camera.

The measurements were conducted using a Canon Tamron Lens with a focal length of 300 mm with a total of 50k fps, and a shutter time of 1 µs. The collected grayscale images are eventually post-processed to identify the vapour jet boundary using Matlab programming tools. More

information in [14]. A schematic of Schlieren setup is shown in Figure 2.

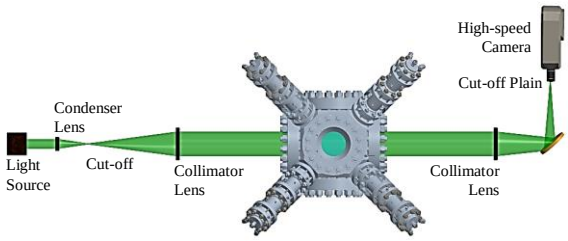

Figure 2. Schlieren Setup

Mie-Scattering:

Three LED arrays are installed crosswise to the chamber and generate a light that is elastically scattered at the surface of liquid droplets, which finally highlights the injection liquid phase. This scattered lights are captured by the same high-speed camera [2] as used for Schlieren imaging. For this measurement, 50k fps with a shutter time of 5 µs have been utilized. A schematic of Mie-Scattering setup is displayed in Figure 3.

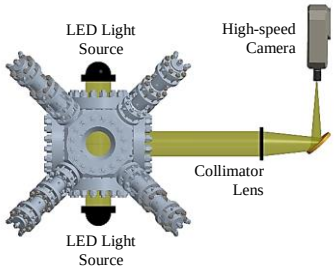

Figure 3. Mie-Scattering Setup

As previously noted, the second section of this research looks at combustion characteristics using a reactive background and two alternative optical techniques. These two techniques fall under the categories of OH* Chemiluminescence and Natural Flame Luminosity.

OH* Chemiluminescence:

OH* Chemiluminescence is an emission of light emitted by the decay of a molecule in an excited state to a lower energy level in a chemical reaction [39]. The exothermic reaction $CH + O_2 \rightarrow CO + OH^*$ is the principal kinetic path for the formation of OH*, and OH* returns to its ground state when this reaction occurs [40, 41].

The OH* signal is an acceptable indicator of the premixed flame and an excellent marker of the high heat release regions [40], which appears in an early reaction step of the mechanism [2] and results from near-stoichiometric high-temperature combustion [42]. This generally happens where the air-to-fuel ratio reaches 1 (near stoichiometric) along the spray perimeter [43, 44]. The intensity of OH* increases rapidly during the intense evolution of combustion following ignition and it is a result of the quick development of the high-temperature reaction region in the premixed combustion zone [44, 45]. In this setup, the light emitted by the radical is filtered (by a band-pass filter with a 307 nm and HBW 25 nm from manufacturer Andover Corporation), and is regarded as indicator for the ignition delay time and the location of FLoL.

In the current study, a high-speed PHOTRON SA-Z camera with a total of 40k fps, a shutter time of 22.5 µs is coupled to a LAVISION high-speed intensifier. Figure 4 depicts the placement of the high-speed camera and intensifier across the CVC.

Natural Flame Luminosity:

The natural flame visible signal is captured by an individual second high-speed PHOTRON SA-Z camera.

Several studies have shown that soot radiation is significantly more powerful than other signals, therefore, it is simple to gather by using natural flame technique [46, 47]. Other chemiluminescence signals, such as OH* and CH*, may be paired with NL; however, the soot signal intensity is so strong that the other signals are inconsequential.

A Carl Zeiss Macro Planar Lens with a focal length of 100 mm is positioned in front of the camera, and visible light is caught with a frame rate of 40k fps, a shutter time of 0.25 µs, and an aperture number of 16. This camera is situated on the right side of the CVC. Figure 4 displays the setup.

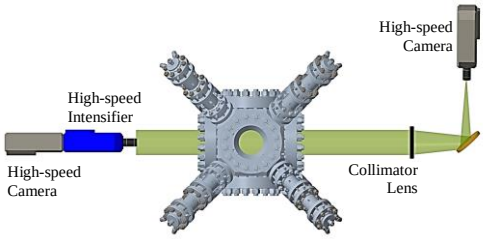

Figure 4. Left Side: OH* Chemiluminescence Setup – Right Side: Natural Flame Luminosity Setup

Jet, Liquid Spray, and Flame Evaluation Methods

The post-processing of Mie-Scattering is based on the intensity value, meaning the residual spray region after removal from the background image is recognised using a constant threshold intensity value. In this case, a value is applied as the minimum intensity threshold for pixels that are interpreted as signal throughout the spray (more information see [48]). In contrast, the image information in Schlieren is dependent on intensity gradients rather than intensity values. Consequently, the overall brightness of the image is immaterial; however, the signal-to-background contrast is crucial. In this post-processing technique, the original image is inverted and subtracted at the first step to reduce the background and increase the contrast of the jet signal. Then, an inverted threshold operation is employed to detect the dark signal caused by the lowest heat input in the spray centre. The Schlieren signal, finally, is produced by merging the last two sub-steps (see [49] and the references therein for more information). References [2, 14, 15, 50] provide more information on Schlieren and Mie-Scattering.

The sole difference between OH*/ natural flame intensity signal post-processings and Mie-Scattering is the intensity threshold type. A constant intensity threshold may result in inaccurate results because the intensity recorded by the camera during the combustion measurement changes gradually from ignition to the end; as a result, an adaptive automatic threshold is chosen and is modified based on the maximum intensity of the image.

Definition of Macroscopic Geometry Parameters

The total penetration S is the distance between the farthest pixel from the nozzle tip and the tip itself. In order to find out the cone angle θ of the jet, the first step is to calculate the intensity centroid, which is the point within line 1. Following this, the half distance between line 1 and the maximum tip penetration is determined (line 2). Straight lines are then fitted over the jet contour between these two lines and the calculated angle is referred as the jet cone angle (Figure 5).

This definition of the cone angle, proposed by the Institute FST of FAU Erlangen-Nürnberg, pertains to the "far-field angle" which is principally influenced by fuel boiling behaviour under evaporation conditions. The term "far-field cone angle" is commonly used in the literatures, but the definition varies [51-53].

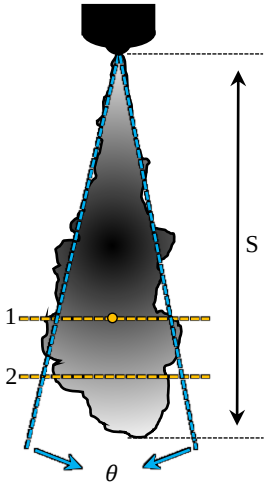

Figure 5. Definitions of the Penetration Length S and Jet Cone Angle θ

Fuels

This paper aims to investigate the spray and combustion behaviours of three various fuel types, including reference diesel, RME, and HVO. Table 1 summarizes the specifications of fuel parameters. The CEC RF-06-03 diesel fuel was utilized as a fossil fuel devoid of FAME components, i.e., pure petroleum diesel. RME is made by esterifying of rapeseed oil, while HVO is produced by hydro-treatment of vegetable oils and/or animal fats. As a result, two generations of bio-diesel have chosen to take part in the study. Note that HVO(S) was used for the spray investigation, whereas HVO(C) was applied for the combustion evaluation. However, both HVOs possess comparable physical features.

Different processes are used to determine the cetane number of fuels. EN ISO 5165 [54] was used for diesel fuel, while DIN EN 17155 [55] was used for HVO(C) and RME fuels. The cetane number target for DIN EN 17155 is based on a CVC, while EN ISO 5165 uses a test engine. The difference in testing protocols makes it unclear how different the final cetane numbers would be if they were all measured the same way. The authors assume that the cetane numbers of RME and diesel are comparable, so only the distinction between low (diesel and RME) and high (HVO) cetane fuels is taken into account.

Table 1. Fuels specifications

	Diesel RF-06-03	RME	HVO(S)	HVO(C)
Density [kg/m3]	834	882.7	765-800	780.3
Lower Heating Value [MJ/kg]	43.2	37.2	- - - -	43.8
Cetane Number [-]	52.4	52.5	70	73
Initial Boiling Point [K]	475.9	Figure 6	Figure 6	Figure 6
Full Boiling Point [K]	633.9	Figure 6	Figure 6	Figure 6
Stoichiometric air-fuel ratio [-]	14.51	12.56	- - - -	14.72
Viscosity (40°C) [mm^2/s]	2.749	4.474	- - - -	3.031

Figure 6 depicts the distillation curves for the employed fuels. Due to the lack of specific data on the RME and HVO distillation curves, information was acquired from a number of sources [27, 56-60].

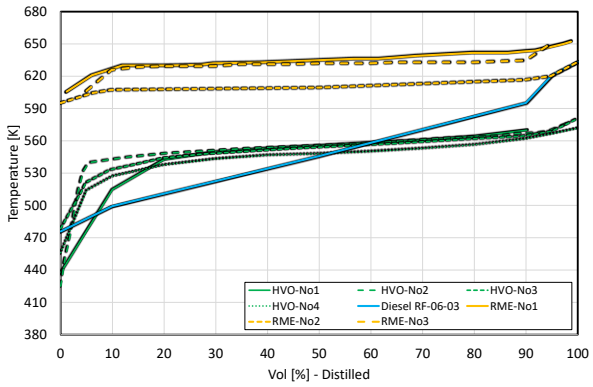

Figure 6. Distillation Curve of the Utilized Fuels (HVO and RME have been collected from [27, 56-60])

The distillation curves of the fuels reveal that RME has a higher boiling point and evaporation does not begin until 590 K; this suggests that, although this fuel has a final boiling point close to that of reference diesel fuel, it is then less volatile. Diesel and HVO have medium distillation ranges, but HVO has a lower full boiling point and evaporates more quickly under identical conditions.

Test Operating Points

This experiment measured seven operating points, three fuels, and two nozzles. Among the parameters already listed in Table 2 for these seven points, variations in chamber (ambient) pressure, chamber temperature, and fuel pressure are visible. In particular, case number 2 serves as a reference point, with each of the other cases differing by a single boundary condition. To offer a thorough picture of the nozzle shape variations, 42 points were ultimately measured and post-processed.

Table 2. Operating conditions

Case No.	Chamber Press [MPa]	Chamber Temp [K]	Fuel Pressure [MPa]
C1	6	873	150
C2	6	923	150
C3	6	973	150
C4	6	923	100
C5	6	923	50
C6	5	923	150
C7	7	923	150

Injectors

Two 300 µm single-hole heavy-duty diesel injectors were utilized for spray and combustion measurements. The injector bodies were produced commercially by Woodward L'Orange GmbH, while nozzles were designed and manufactured in a prototype manner. These injector types are commonly utilized for fuel injection systems in a variety applications, including power generation and large industrial engines which are typically used in marine, locomotive, trains, and oil rigs.

As seen in Table 3, the K factors and length to diameter ratio of these two injectors differ.

The K factor is determined by the following formula:

$$\boldsymbol{K} = \frac{\boldsymbol{d_i[\mu m] - d_o[\mu m]}}{\boldsymbol{10}} \quad (1)$$

d_i is the nozzle entrance diameter and d_o is the nozzle exit diameter.

The first injector is a conical nozzle representing 1.3 mm in length, while the second injector is a cylindrical nozzle with a length of 0.65 mm. Figure 7 shows a schematic depiction of these two nozzles. As mentioned in the literature section, the previous studies have reported contrasting results regarding the combustion development

of various nozzles, which can be explained due to the larger variations in the geometry of the selected injectors [11-13]. However, the current study has made an effort to select the injectors with the fewest variety of geometries. Therefore, two parameters including cavitation formation and minimal geometry variations were the primary criteria for choosing these two nozzles. Generally speaking, compared to the conical shape, the cylindrical nozzle shape and the shorter nozzle length both produce more cavitation.

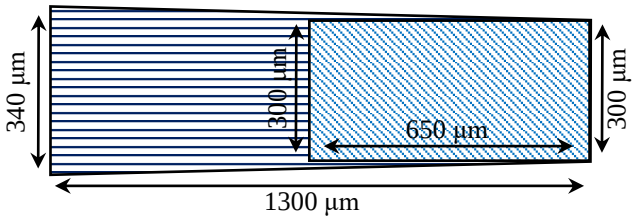

Figure 7. Dimensions of Two Injectors, Black Horizontal Lines: Conical Nozzle. Blue Downward Diagonal Lines: Cylindrical Nozzle.

Table 3. Nozzles Specifications

Parameters / Nozzles	$\emptyset_{entrance}$ [µm]	$\emptyset_{exit}$ [µm]	Length [mm]	L/D [--]	K factor [--]
Conical	340	300	1.3	4.33	4
Cylindrical	300	300	0.65	2.16	0

A comparison of the mass flow rates of two nozzles is shown in Figure 8. The HDA MOEHWALD mass flow measurement device was used to calculate the mass flow rate (German: "Hydraulisches Druck-Anstiegsverfahren"). The idea behind the device is to detect a rise in hydraulic pressure, which occurs when fuel is introduced into a particular filled volume. Thanks to a speed of sound sensor. In addition to the device basic design, the boundary conditions can be modified, including the fuel pressure, injector body temperature, and chamber pressure. In this measurement, cases 1 and 3 are neglected since chamber temperature change is not a relevant situation for mass rate measurement. The outcomes of these two points must coincide with the reference point result (case number 2).

In general, increased mass flow rates of the conical nozzle are visible at each of the aforementioned measurement sites. This nozzle has roughly 15% higher mass flow rate than the cylindrical nozzle.

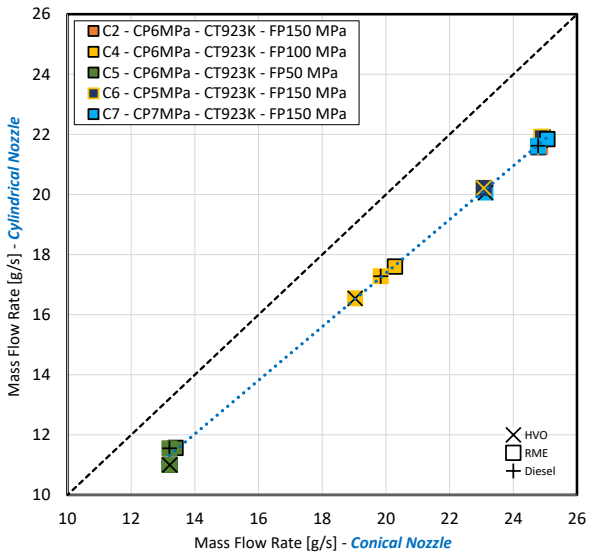

Figure 8: Mass Flow Rate [g/s] – Cylindrical and Conical Nozzles

Jet Penetration Theory

Utilizing jet theories and momentum flux conservation, researchers have developed and refined a fundamental 1D model for the stationary injection process. Check the cited sources for further details [16, 19, 20, 61]. They developed a model capable of describing the relationship between jet penetration length and nozzle shape, fuel, and air

conditions. This model is applied to fully developed jet based on the following assumptions:

1. A rectangular profile of the spray velocity at each distance x from the nozzle exit.
2. The movement of entrained ambient gas outside the spray is normal to the spray axis.
3. Constant nozzle exit velocity (without throttle effects at injection start), constant spray cone angle, and constant discharge coefficient.
4. Air flows around the spray under no-slip conditions (between fuel and ambient gas).
5. Even in the mixture, the ambient gas density remains constant.
6. Constant mass flow rate of fuel regardless of nozzle distance.

Desantes et al. [61] integrated X-ray observations for two distinct nozzles and published the physical considerations-based theoretical development. They demonstrated that under the assumption of a radial Gaussian distribution of velocity and mass in the far field of the nozzle, the momentum balance formulas are equally valid.

On the basis of the model of Naber and Siebers [20], the axial flow can be characterised by the conservation of momentum. It is assumed that the initial momentum issued by the nozzle is constant at any position x along the spray leading to the nozzle tip (equation 2).

$$\dot{M}_0 = \dot{M}(x) = constant \tag{2}$$

The outlet momentum flow of the nozzle is characterised by the mass flow rate and velocity of the fuel. Consequently, equation 2 can be transformed into the next equation (3). Due to air entrainment into the spray immediately after fuel exits the nozzle, momentum flow can be viewed as the sum of air and fuel mass flow rate along the axial distance x with a common velocity u(x).

$$\dot{m}_f . u_o = \left(\dot{m}_f + \dot{m}_a(x)\right) . u(x) \tag{3}$$

$\dot{m}_f$ is the fuel mass flow rate, $\dot{m}_a$ is the air mass flow rate, and u_0 is the initial jet velocity. As previously stated, the model assumes complete momentum conservation through injection; hence, the total jet penetration can be calculated by solving the above equation for the spray [20].

$$S = \left(\frac{C_v \times (2 \times C_a)^{0.5} \times d_o \times t}{a \times \tan(\theta/2)}\right)^{0.5} \times \left(\frac{(P_f - P_a)}{\rho_a}\right)^{0.25} \tag{4}$$

S is the total penetration, a is a calibration constant, θ is the cone angle, C_a is the area contraction coefficient, C_v is the orifice velocity contraction coefficient, t is time from start of injection, P_f and P_a are fuel and air pressure, respectively, and ρ_a is the air density. The cone angle θ of the above equation is calculated from Schlieren image (jet phase of injection).

The orifice velocity contraction coefficient is associated to the area contraction coefficient (flow rate loss due to cavitation and non-uniform velocity profiles at the orifice exit) and the discharge coefficient. The following equation illustrates this connection [20].

$$C_d = C_a \times C_v \tag{5}$$

With:

$$C_a = \frac{A_{effective}}{A_{theory}} \quad (6)$$

$$C_v = \frac{v_{effective}}{v_{theory}} \quad (7)$$

The area covered by the liquid fuel is represented by $A_{effective}$. The amount of vapour present at the nozzle exit has a direct influence on the area contraction coefficient, making it a crucial parameter for quantifying cavitation [62]. The findings of [7, 10] demonstrate that the area coefficient C_a drops when cavitation occurs, as cavitation forms a vapour phase at the injector hole outflow section. As a result, the liquid phase effective area is diminished.

The velocity at the exit of the nozzle is denoted by $v_{effective}$. This is inversely proportional to cavitation because cavitation reduces the cross-section of the liquid phase at the output section of the hole. The velocity coefficient C_v rises as the level of cavitation increases [7, 10].

In addition, the discharge coefficient can be defined as follows:

$$C_d = \Delta m \Big/ (\Delta t \times A_o \times \rho_f \times \sqrt{2 \times \frac{P_f - P_a}{\rho_f}}) \quad (8)$$

Δm is the total mass of fuel injected within the injection duration Δt and A_0 is determined by the nozzle exit diameter. It is the ratio between the actual mass and the theoretical maximum injected mass.

Under non-cavitating conditions, the mass flow rate is proportional to the square root of the pressure drop across the nozzle; however, once cavitation occurs, there is no longer direct relationship between the mass flow rate and pressure drop. It indicates that a reduction in back pressure cannot enhance the mass flow rate [7]. Cavitation can reduce the wall shear stress within the nozzle when it occurs between the liquid phase and the hole wall. In conclusion, cylindrical nozzles have a lower area contraction coefficient and less wall shear stress within the nozzle, which results in a higher effective cavitation velocity at the same pressure drop [7, 9].

When equations 4 and 5 are considered, the relationship between jet penetration and injection parameters can be expressed as:

$$S = \left(\frac{\dot{m}_f \times t \times 1000}{a \times tan\left(\theta/2\right) \times d_o \times \pi/4}\right)^{0.5} \times \left(\frac{1}{C_a \times \rho_a \times \rho_f}\right)^{0.25} \quad (9)$$

In which jet penetration is proportional to the parameters listed below:

$$S = f(\dot{m}_f{}^{0.5}, C_a{}^{-0.25}, a^{-0.5}, \tan\left(\theta/2\right)^{-0.5}, d_o{}^{-0.5}, t^{0.5},$$

$$\rho_a{}^{-0.25}, \rho_f{}^{-0.25}) \quad (10)$$

This correlation demonstrates that only the fuel mass flow rate has a direct effect on jet penetration depth, but the other factors, including air/fuel density, nozzle diameter, cone angle, and area contraction coefficient have inverse effects.

Fuel/air ratio versus time can be theoretically determined using the following formulae. These equations establish the relationship between the amount of fuel and air at any axial distance.

$$\frac{\dot{m}_f}{\dot{m}_a} = \frac{2}{\sqrt{1+16\tilde{x}^2}-1} \quad (11)$$

Which $\tilde{x}$ is:

$$\tilde{x} = S \times a \times tan\,\frac{\theta}{2} \times C_a^{-0.5} \times d_o \times \left(\rho_f/\rho_a\right)^{-0.5} \quad (12)$$

This equation could well be rewritten as follows:

$$\frac{\dot{m}_f}{\dot{m}_a} = 0.5 \times \left(\frac{C_a \times \rho_f}{\rho_a}\right)^{0.5} \times \frac{d_o}{S \times a \times \tan(\theta/2)} \quad (13)$$

The final correlation between fuel/air ratio and injection parameters can be expressed below:

$$\frac{\dot{m}_f}{\dot{m}_a} = f(S^{-1},\ {C_a}^{0.5}, {\rho_f}^{0.5}, {\rho_a}^{-0.5}, a^{-1}, \tan(\theta/2)^{-1}, d_o) \quad (14)$$

The link between jet penetration and injection parameters (10) is utilized to characterise the impact of measurement operating points on jet penetration data, whereas equation 13 is explicitly derived to explain the air-to-fuel ratio at various axial locations.

The correlation between jet parameters and air entrainment is finally rewritten as follows [20]:

$$Air\ Entrainment \propto (\rho_a, d_o, u_f, tan\,\frac{\theta}{2}) \quad (15)$$

According to the equation above, factors such as air density, jet cone angle, and nozzle diameter directly affect the amount of air entrainment, while fuel velocity which is influenced by orifice velocity contraction coefficient, fuel mass flow rate, fuel pressure, and fuel density is accelerating air entrainment, but the air-to-fuel ratio at different axial distances stays constant.

Results and Discussion:

One of the differentiating features used to determine spray behaviour, the initiation and propagation of combustion, and the characteristics of emissions is the nozzle geometry [8, 17, 63-65]. Therefore, the current research links the nozzle characteristics to the initial preparation of the mixture and the progression of combustion, which are divided into the main two sections below.

The first section introduces jet and liquid spray parameters obtained in an inert gas background and associates nozzle geometry to mixture formation and air entrainment process. Several experimental parameters are employed in this section, including jet and liquid spray penetration lengths, cone angle, projected cone area, and computed air-to-fuel mass ratio.

The results of the inert parameters are connected to the combustion post-processed data in the second section, which further includes ignition delay, soot formation time, and FLoL.

Jet and Liquid Spray Parameters – Inert Gas Background

In the current section, the effects of chamber and fuel test conditions are evaluated and clearly illustrated in each figure of the results, which helps to find out jet and liquid spray behaviours in an inert gas background. These effects are in addition to the general differences between the two nozzles, which will be shown in details later.

Conical nozzle results in each figure are correlated with the abscissa axis, while cylindrical nozzle results are associated with the ordinate axis. Each rectangle point is connected to one of the operating points and displayed in a recognisable manner to facilitate a better comprehension of the implications of varied operating conditions. Taking into account the reference point, it is feasible to divide all

operating points into three groups: the influence of chamber temperature, chamber pressure, and fuel injection pressure.

Figure 9 shows the time-averaged liquid spray penetration of two nozzles to that of all sites. This figure has been divided into three levels to provide a clearer illustration of the results. It shows the variation in chamber temperature at the top and the variation in chamber pressure at the bottom. It should be noted that the highest air temperature with HVO fuel was experimentally missed in this section.

As previously mentioned, the chamber temperature is increased from 873 K to 973 K while all other conditions remain unchanged. In general, a higher chamber temperature accelerates the evaporation rate, which shortens the time that liquid spray penetration lasts. This indicates that the fuels and nozzles specified go through a quicker change from liquid to vapour phase (Figure 9). Additionally, the influence of variations in chamber gas density on liquid spray penetration is not negligible. More gas is pushed into the spray plume by higher density at lower temperatures, which increases the amount of instantly available energy for evaporation.

Figure 9 ought to demonstrate a relationship between rising chamber pressure and correspondingly falling liquid spray penetration. The maximum liquid spray penetration and the amount of energy available for the evaporation are, in general, always correlated. Additionally, a steeper droplet deceleration brought on by an increase in aerodynamic drag on the droplet may result in a shorter liquid spray penetration. As a result, as can be seen in this figure, the pressure of the surrounding gas affects the total liquid spray penetration.

It will be shown later in this section that fuel pressure has no impact on the mass ratio (air-to-fuel mass ratio at different axial locations) since it has no impact on the jet cone angle. Therefore, at different injection pressures, it is reasonable to infer that the phase transition from liquid to gas happened earlier but at the same distance from the nozzle outlet [66]. Although, various injection pressure has an effect on the early spreading phase of temporal development of liquid spray penetration depth [15], but it is not demonstrated here since the displayed quantity is only associated to the maximum quasi-steady phase of liquid spray.

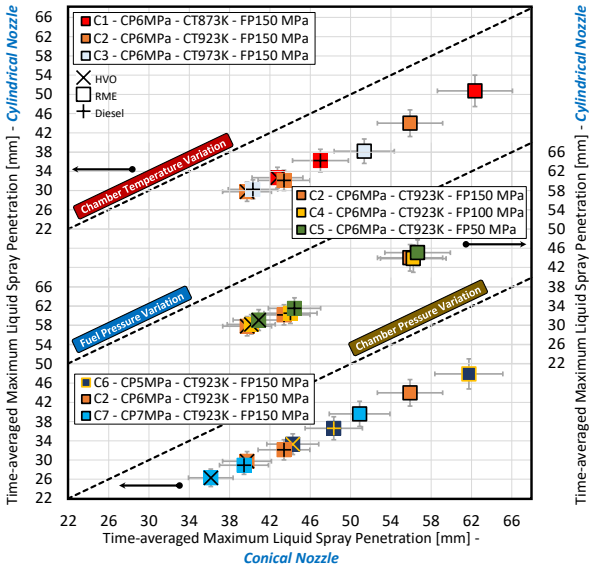

Figure 9: Time-averaged Maximum Liquid Spray Penetration [mm] – Cylindrical and Conical Nozzles

The site of phase transition as well as the temporal and spatial behaviour of evaporation are precisely controlled in accordance with the distillation behaviour, and the liquid spray penetration grows as the (full) boiling point rises.

Figure 6 showed that the total boiling point of RME is higher and that evaporation does not really start until temperature is higher than 590 K. In other words, even though this fuel has a complete boiling point close to that of diesel, it is predicted to be the least volatile and has the longest liquid spray length. HVO, on the other hand, should evaporate more quickly than diesel due to its lower full boiling point.

Figure 9 makes the distinctions between the fuels quite evident. The general behaviour of the shortest liquid length of HVO and the longest liquid length of RME may very well be separated if a single experiment point (Table 2) is observed throughout the figure. The absolute amount of the difference between the operating points is not the same for all fuels due to the reason that factors such as total boiling point and distillation curve, which have a big impact on liquid evaporation, can change under different boundary conditions.

In a quasi-steady phase of injection development, Figure 10 shows a time-averaged far-field vapour cone angle. In general, there were no notable differences between various operating points, however the cone angle may vary slightly under different operating conditions. Numerous investigations have demonstrated that neither the chamber temperature nor the air or fuel pressures influence the jet cone angle [15, 66]. For instance, Riess et al, [15] proved that the cone angle is the same for a passenger-car injector working in the temperature range of 873 to 973 K.

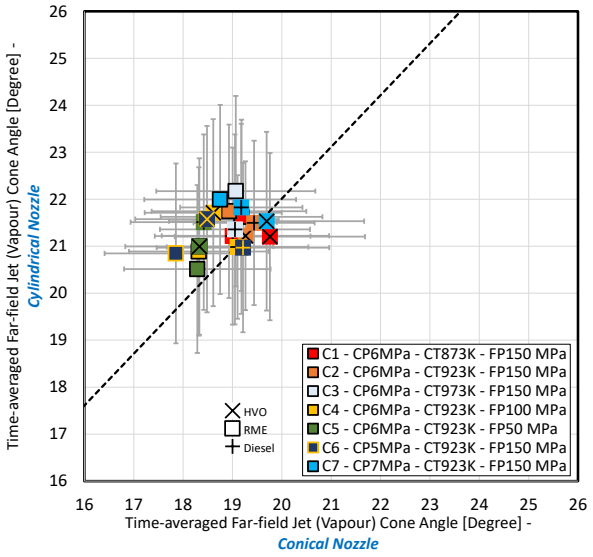

Figure 10: Time-averaged Far-field Jet (Vapor) Cone Angle [Degree] – Cylindrical and Conical Nozzles

Figure 11 compares two nozzles in terms of the time it takes to achieve a jet penetration length of 75 mm. This figure displays the time due to the consistent development trend and the constant behaviour of the jet expansion at various sites. Referring to the final correlation of Naber and Siebers [20], there is no direct effect of temperature on jet penetration; rather, temperature indirectly affects jet penetration as a result of changes in chamber gas density ($S \propto {\rho_a}^{-0.25}$). Although, for the range of recorded gas temperatures, the influence of density change is not substantial, a slight variation is anticipated and could be observed in Figure 11. The density of ambient gas (Nitrogen) varies from 22.64 kg/m^3 at 873 K and 21.49 kg/m^3 at 923 K to 20.34 kg/m^3 at 973 K.

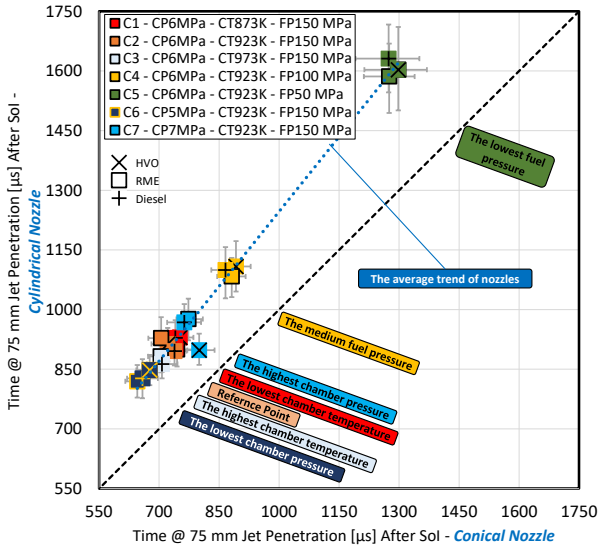

Figure 11: Time @ 75 mm Jet Penetration [µs] after SoI – Cylindrical and Conical Nozzles

The chamber pressure is increased from 5 to 7 MPa and the pressure of 6 MPa is the reference case point. At 5 MPa, the density of ambient gas is 17.97 kg/m3, at 6 MPa it is 21.49 kg/m3, and at 7 MPa it is 24.98 kg/m3. Referring to equation 10, the sole variable related with the air pressure change is the air density ($S \propto {\rho_a}^{-0.25}$). The extent and relevance of the ambient density shift in relation to the ambient pressure change is greater and more pronounced than in the part before, where the gas density was not significantly changed. Without a reduction in local spreading velocity and associated suppression of penetration length, no other explanations could adequately explain how density affects jet penetration. This is due to the fact that the initial momentum flux is maintained throughout the growth of the jet, and the total penetration depends on the conservation of momentum between fuel and air.

The equation 10 covers some of the other various effects of injection pressure, such as fuel mass flow rate and fuel density ($S \propto {\dot{m}_f}^{0.5} \propto {\rho_f}^{-0.25}$). Although the effect of injection pressure on any rise of fuel density is potentially ignorable, a higher fuel pressure produces a larger fuel mass flow rate and actually causes a longer penetration length per unit of time.

Fuel pressure, on the other hand, has no detectable impact on fuel density, and the individual densities of diesel, HVO, and RME fuels are only marginally different. Theoretically, this might affect jet penetration, but the impact would be minimal. Figure 11 shows all fuels in close proximity as they are all being tested under the same conditions.

Numerous studies have discovered that cavitation behaviour depends on fuel type, chamber pressure, and injection pressure [1, 6, 7, 10]. Increasing cavitation in a cylindrical nozzle causes a wider jet cone angle at the nozzle exit due to greater turbulence and different velocity profiles. The bigger cone angle of the cylindrical nozzle is maintained at all measured sites, and variations in cone angle between various boundary conditions and fuels can be disregarded (Figure 10). The effect of different mass flow rates between nozzles, on the other hand, might be neglected if the influence of injection pressure on cone angle is taken into account since mass flow rates have no impact on cone angle. Therefore, it is reasonable to conclude that the only factor affecting the cone angle in this situation is the geometry of the nozzle. The average cone angle of the cylindrical nozzle is roughly 13% greater than that of the conical nozzle.

The wider cone angle of the cylindrical nozzle, on the first side, guarantees that more air is brought into the spray plume, increasing the energy available for fuel droplet

evaporation. On the other side, the mass flow rate of the cylindrical nozzle is around 13% (at various points) less than that of the conical nozzle. The maximum liquid spray penetration is directly related to the fuel mass flow rate and available energy for evaporation; hence, the cylindrical nozzle has less liquid spray penetration than the conical nozzle (Figure 9).

The conical nozzle has a longer jet penetration length than the cylindrical nozzle, as seen in Figure 11. This is accomplished by increasing the mass flow rate and decreasing the cone angle of the conical nozzle.

For the purpose of demonstrating a larger cone area of the cylindrical nozzle, the projected jet cone area is post-processed and extracted from the collected images. This cone area, which is measured once the jet penetration reaches 75 mm, is compared in Figure 12. The cylindrical nozzle has a greater area at each test point.

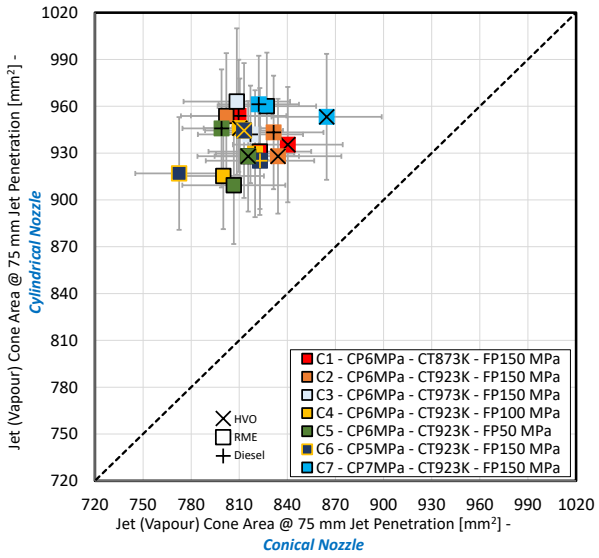

Figure 12: Jet (Vapour) Cone Area @ 75 mm Jet Penetration [mm^2] – Cylindrical and Conical Nozzles

In diesel-type engines, the mixture is formed as soon as the injection phase begins and lasts until the fuel has been completely burned. The fuel and environmental conditions may speed up, slow down, or have an individual impact on the quality of mixture formation processes such as atomization, evaporation, and air entrainment.

The mixture formation is closely related to the mass ratio of air-to-fuel at each axial position. Theoretically, the air-to-fuel mass ratio can be determined using Naber and Sieber's 1D model [20]. The model reliable estimation of entrained air enables a comprehensive knowledge of mixture formation in both nozzles.

Three potential scenarios for the air-to-fuel mass ratio are shown in Figure 13. Three levels of penetration length, 25 mm, 50 mm, and 75 mm, were used in the first scenario and were indicated by rectangular dots. Each point is displayed plainly and correlates to a test point, similar to earlier iterations. The second scenario is illustrated with post-processed data at various time steps ranging from 200 to 1600 µs with a 200 µs step. Due to the fact that multiple points were paired when various time steps were analyzed, a polynomial trendline was drawn through all points and is depicted as a line in this figure.

In contrast to the second scenario, the cylindrical nozzle takes longer to travel the same distance, and the jet cone area widens at all points, thus the overall trend of the air-to-fuel mass ratio tends to be closer to the cylindrical nozzle. As a result, the average behaviour shifts more in favor of the cylindrical nozzle. Figure 12 already showed

the cylindrical nozzle wider cone area at the same penetration length.

The third scenario involves maintaining the same injected fuel mass while obtaining the air-to-fuel ratio. In other words, these statistics are derived in both nozzles when they both achieve the identical fuel mass. Similar to the second scenario, a linear line is passed through all point between 0.5 and 26 mg with a step of 1 mg (except from the beginning, which starts from 0.5 to 1 and then 2 mg). Through the utilization of this scenario, the impact of the nozzle varying mass flow rate on the air-to-fuel ratio is completely eliminated.

From the perspective of mixture formation, a change in fuel mass flow rate has no impact on air entrainment or mixture formation, as a bigger mass ultimately results in more air being entrained into the spray plume while the air-to-fuel ratio stays unchanged. In this case, both air and fuel momentum fluxes increase at the same magnitude with injection pressure change. This is plainly monitored by the air-to-fuel ratio at varying fuel pressures, which are typically close to one another. Additionally, previous study proved that an increase in nozzle exit velocity and atomization quality do not impact the air entrainment process [67], hence, injection pressure cannot alter air-to-fuel ratio and only speeds up the mixture process. This result is an agreement with previous study [14].

In addition, the overall amount of air entrainment in the whole of spray development is impacted by chamber gas temperature. In a small-scale passenger cars injector, Riess et al. [2] utilized Raman Spectroscopy measurement and proved that the chamber temperature has no direct influence on mixture distribution. However, in larger-scale injector, a positive influence can be visualized and it appears to be non-negligible. To put it another way, the authors are arguing that when high mass flow rate nozzles are used, the influence of some boundary conditions that had little to no effect on spray and combustion in passenger-car injectors are intensified and appeared to have a bigger impact in heavy-duty injectors. The authors continue the measurements of the heavy-duty injectors using a Raman Spectroscopy to shed more lights upon the mixture formation in different gas temperature.

The major influence is made up of the change in chamber gas pressure, which has the greatest effect on the amount of entrained air.

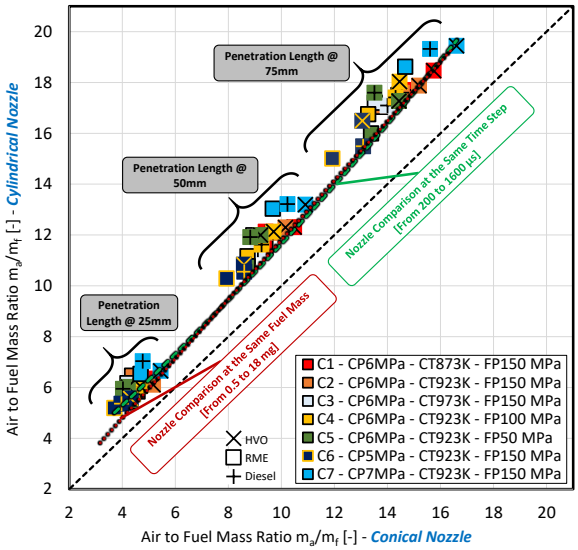

Figure 13: Air-to-Fuel Mass Ratio m_a/m_f [-] - Cylindrical and Conical Nozzles

From a nozzle geometry standpoint, a rise in cavitation increases the effective nozzle exit velocity [7, 10]. It could be assumed that the cylindrical nozzle incorporates more air into the spray. The comparison of all scenarios demonstrate a greater amount of air entrained in the cylindrical nozzle.

Figures 14 and 15 display qualitative jet and liquid spray boundaries compared for diesel fuel at the reference position, respectively. Notably, all measurements were repeated 32 times, and the most recent statistics presented indicate the mean of these repetitions. However, Figures 14 and 15 combine 32 injection outlines to illustrate the maximum and minimum injection boundaries at a single location. The results demonstrate that the conical nozzle has more jet and liquid spray penetration, whereas the cylindrical nozzle has a greater jet cone angle.

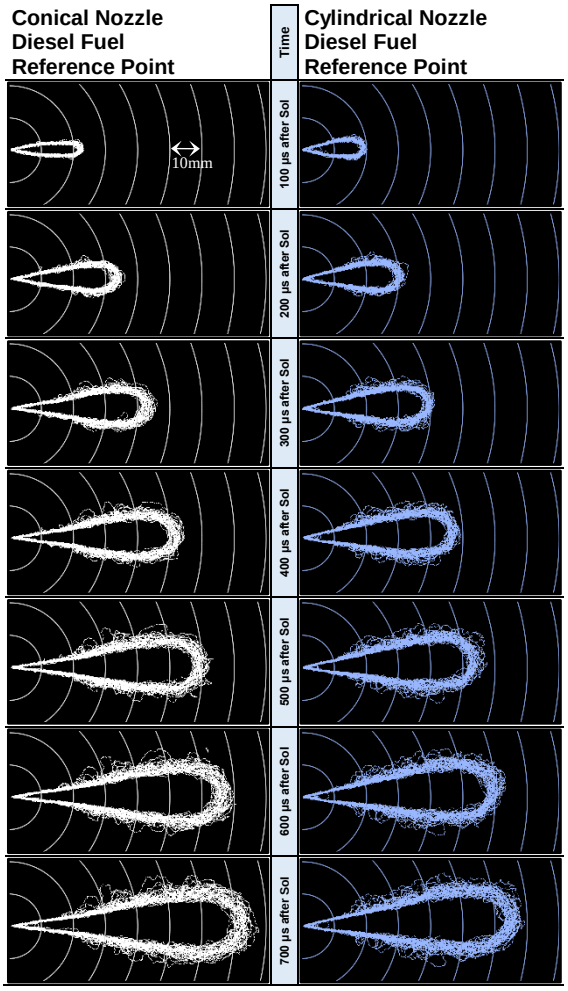

Figure 14. Jet Boundaries of 32 Injections at the Reference Point (Table 2) Using Diesel fuel

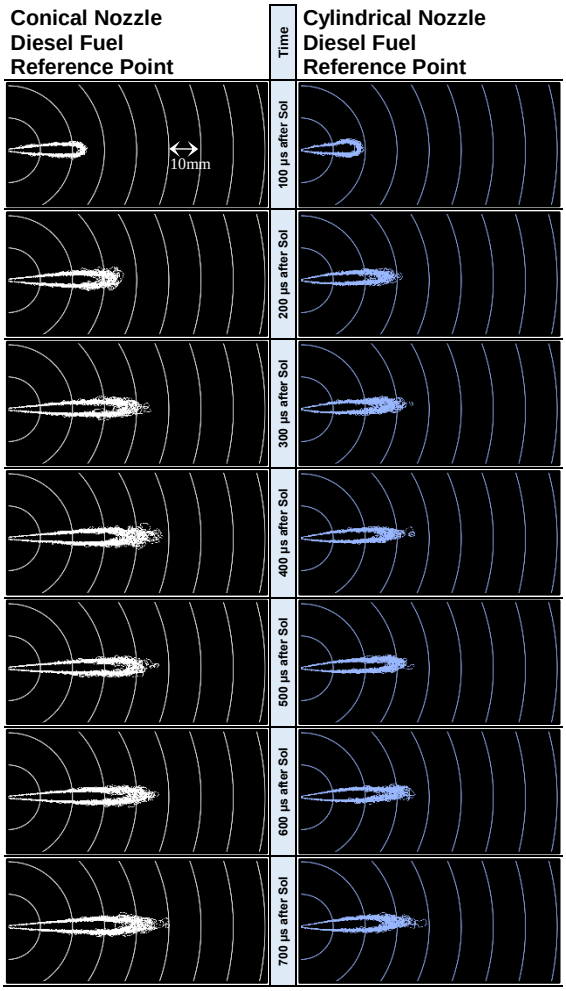

Figure 15. Liquid Spray Boundaries of 32 Injections at the Reference Point (Table 2) Using Diesel fuel

Important insights are gained from the spray parameters, such as the finding that liquid spray penetration remained constant over a wide range of injection pressures but shortened with an increase in chamber temperature and pressure. While HVO boiling point caused the liquid to evaporate more quickly, RME higher boiling point allowed for the longest liquid spray penetration. Moreover, the results showed that chamber temperature only indirectly affects jet penetration (through variations in chamber gas density). The change in density when chamber pressure is altered is also showed as the only correlated variable that influences jet penetration. A higher fuel pressure leaded to a greater fuel mass flow rate

and resulted in a longer penetration length per unit of time. The slight variations in fuel density had a small impact on the overall jet penetration as well. Under different operating conditions, the jet cone angle also did not change significantly.

Higher cavitation in the cylindrical nozzle resulted in a wider jet cone angle and ensured that more air is introduced into the spray plume, increasing the energy available for fuel droplet evaporation. However, since the cylindrical nozzle has a lower mass flow rate than the conical nozzle, liquid spray penetration in this injector remained at a lower level. On the other hand, these two factors directly affected the conical nozzle higher jet penetration. The ability of the cylindrical nozzle to create higher air entrainment and prepare faster initial stoichiometric region was demonstrated by comparing various air-to-fuel mass ratio scenarios. The ratio is generally a significant parameter to describe the behaviour of combustion initiation and propagation.

Ignition and Combustion Parameters – Reactive Gas Background

Ignition Delay Time and the Flame Lift-off Length

The current part uses dry air as a reactive gas to describe the behaviour of the flame in a reactive environment. The ignition delay time, soot appearance time, and FLoL are the most significant combustion characteristics covered in this section.

The theoretical ignition delay time is made up of two unique time delays: the physical delay time and the chemical delay time. These delays cannot be distinguished from one another since they occur simultaneously. Physical characteristics of fuel and chamber conditions dictate physical delay time, which is a time summation of atomization, evaporation, and air-fuel mixing [68]. Chemical delay time is the interval between the availability of an ignitable amount of fuel vapours and the stimulation of the activation energy of the reactions [23].

As was already mentioned, the initial intensified OH* signal captured by a high-speed camera is referred to as the ignition delay. The first ignition region cannot be detected as the ignition delay since it does not correlate to the ignition of all recorded injection shots. According to statistics, the initial OH* signal appears at various initial time steps in 32 injections, but within a small time window. This study bases its calculation of the ignition delay on a cumulative Gaussian distribution over the initial ignition signals [2]. The formulation is described by the following mathematical equation:

$$F(x) = \frac{1}{\sigma\sqrt{2\pi}} \int_{-\infty}^{x} e^{-0.5\left(t-\mu/\sigma\right)} dt \quad (16)$$

The expected value μ leads to the maximum probability density and is ultimately regarded as the ignition delay, while σ is the standard deviation around the expected value of ignition.

In the same manner as before, all combustion parameters are compared between two nozzles, with the cylindrical nozzle on the ordinate axis and the conical nozzle on the abscissa axis.

The results of each ignition delay are defined and shown in three independent levels in Figure 16. Repeating the reference point inside each category makes it easier to understand how the points differ. The development in each category from the smallest to the longest ignition

delay time generally follows a pattern: from 873 K to 973 K for chamber temperature variation, from 150 MPa to 50 MPa for fuel pressure variation, and from 7 MPa to 5 MPa for chamber pressure change.

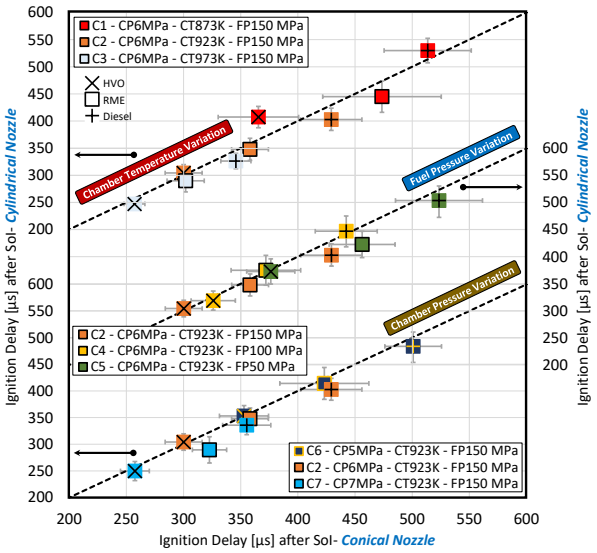

Figure 16. Ignition Delay Time [µs] after SoI – Cylindrical and Conical Nozzles

The ignition delay trend of the first category (chamber temperature variation) demonstrates both physical and chemical impacts. Rapid liquid evaporation, which speeds up the formation of a homogenous zone, is the first effective parameter and influences directly the physical delay time. The fuel chemical reaction, which is strongly impacted by the ambient temperature, is the subject of the second explanation. When the temperature rises, the chemical reaction time lowers, resulting in an increase in Damköhler Number (the ratio of characteristic liquid residence time to characteristic chemical reaction time) [23, 69]. A higher Damköhler Number denotes a quick forward reaction, whereas a lower value implies a kinetically regulated response. Through previous research, Khan et al. [23] showed that the relationship between the chamber temperature and the ignition delay time is exponentially inversely proportional; a similar relationship is shown in Figure 16.

The variation in fuel mass flow rate in the following category indicates the impact of fuel pressure on ignition delay. The time needed for initial fuel evaporation and subsequent mixture preparation increases as fuel flow rate falls; as a result, ignition happens later. The quality of the mixture produced cannot potentially be affected by changing mass flow rates, as was covered in great detail in the preceding section; nonetheless, the time needed to produce the mixture is longer at lower fuel pressures.

The third category explores towards how chamber pressure affects the incidence of an ignition. Increased chamber pressure appears to accelerate the occurrence of ignition, according to the general trend. Higher density speeds up the creation of the stoichiometric area and reduces the ignition delay time by increasing the volume of air entrained into the spray plume and enhancing fuel evaporation. Researchers have also noted that a higher chamber pressure increases chemical kinetics, leading to a quicker ignition [70]. Higher chamber pressure raises the Damköhler number due to a greater diffusional barrier to fuel vapour spread (which lengthens residence time), and a longer reaction time [23].

In the literatures, the relationship between ignition delay and chamber pressure is introduced as ($ID \propto {}^{1}/_{P_a^b}$) and it was proved that this relationship holds true for a wide

variety of fuels [23]. b is a constant value and the same trend can be visualized in Figure 16.

Figure 17 depicts a comparison of all ignition delay points. The following is a list of the standard variables that influence this parameter between fuels and nozzles:

1- Fuel cetane number: The value of this number, which gives an indication of the combustion speed at which diesel-type fuel burns, can be used to estimate how quickly a fuel starts to burn. HVO has the highest cetane values, while RME and reference diesel have the lowest.

2- Preparing the initial stoichiometric zone, which is essential to produce the subsequent ignition kernels, is one of the most effective methods for initiating the ignition. RME is the only fuel that contains close to 10% oxygen and creates well-mixed zones more quickly than other fuels.

3- Ignition could well be directly affected by fuel distillation behaviour. In fact, faster evaporation causes stoichiometric zones to expand more quickly, which could speed up the ignition rate.

4- In the end, the type of nozzle geometry affects the initial mixture formation, fuel mass flow rate, liquid spray penetration length, and jet cone angle, all of which can affect the start of an ignition and the spread of a flame.

Cetane number, oxygen concentration, liquid spray penetration, and air entrainment all have a trade-off influence on ignition time when the aforementioned variables are combined. Diesel and RME: since diesel fuel has a low cetane number, its ignition takes longer than that of other fuels. RME fuel burns more quickly than diesel even if they both have the same cetane value. The main factor is the 10% oxygen content of RME components, which accelerates the well-premixed mixture and results in early first ignition kernels. Diesel and HVO: in terms of liquid spray length and distillation curve, these two fuels should ignite identically, however HVO ignites more quickly because of its greater cetane number.

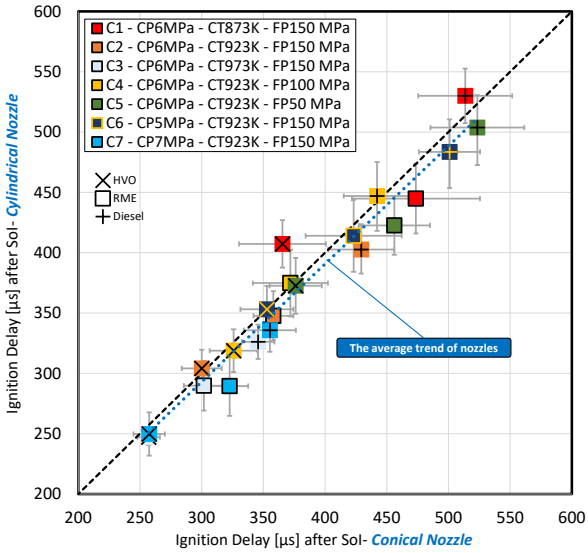

Figure 17. Overall Ignition Delay Time [µs] after SoI – Cylindrical and Conical Nozzles

The cylindrical nozzle can rapidly evaporate fuel owing to its cavitation process and larger turbulences at the nozzle hole exit. It can also deliver much more air to the spray plume thanks to its wider cone angle. Furthermore, Figure 13 showed that under different conditions, the level of air in the spray region is higher in the cylindrical nozzle, which contributes to a quicker igniting. The ignition delay

time is typically decreased by 4.5% (on average) as a result of the cylindrical nozzle igniting faster (Figure 17).

This nozzle trend is in agreement with the previous study [13] but in contraction to [11, 12]. All nozzle geometries, including exit diameter, conicity, and length, as well as nozzle mass flow rate, have direct effects on the formation of the initial air-to-fuel stoichiometric area, which in turn determines the ignition delay time. This is the main reason why researchers have discovered distinct conical and cylindrical nozzle patterns.

Apart from the ignition delay, FLoL is generally considered as a remarkable parameter since the amount of air-to-fuel premixing upstream of the FLoL, could influence the combustion, the composition of the reactants, and soot formation downstream of the spray [36, 37, 68]. As a result, the remaining soot production downstream will therefore be influenced by the way the air reacts during the diffusion flame as well as by the amount of air entrained to the flame downstream of the FLoL [68]. Usually, longer FLoL marks more entrainment of fresh air into the spray jet which leads to a leaner combustion [69].

The FLoL is determined using high-temperature chemiluminescence signal of an excited-state OH (OH*). This length influences and correlates with combustion behaviour and soot formation during the mixing controlled phase of combustion. Siebers et al. [21, 22] developed an empirical power-law correlation for the FLoL of diesel spray that takes into account a number of parameters:

$$FLoL = f(T_a^c,\ \rho_a^d,\ u_f^e,\ Z_{st}^f,\ d_o^g) \qquad (17)$$

e and g are positive constants and c, d and f are negative constants. They are tuned according to the testing conditions and fuel used [46, 71]. T_a is chamber temperature, u_f fuel injection velocity, and Z_{st} chamber oxygen concentration.

The following is the relationship between Z_{st} and the stoichiometric air-to-fuel ratio f_s: This is related directly to the oxygen concentration within the chamber.

$$Z_{st} = {}^{1}/_{(1 + f_s)} \qquad (20)$$

The FLoL is often divided into two stages; the initial length is acquired from to the first ignition kernels, and the second length, which is approximately constant, is obtained from virtually quasi-steady phase. The first region varies significantly with test repetition due to statistically significant differences in initial ignition location, whereas the average trend of the second zone is repeatable. The information reported in this study is therefore considered to be an average FLoL quasi-steady

state. Figure 18 shows and compares the FLoL of all measurement points.

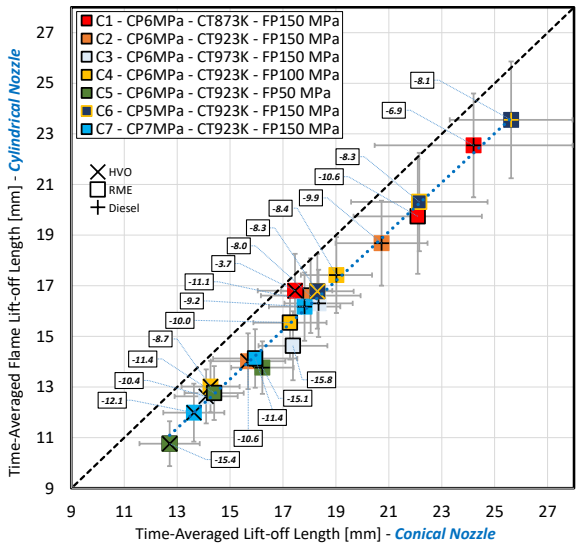

Figure 18. Time-averaged Flame Lift-off Length [mm] – Cylindrical and Conical Nozzles

The relationship between the FLoL and chamber temperature shown in Figure 18, is consistent with previous observations [47, 72]. Although shorter liquid length at higher temperatures also contributes to this tendency, faster ignition of the initial air-to-fuel mixture is the primary factor causing lower FLoL. It is worth to mention that the liquid length is always shorter than the FLoL.

The ignition delay time versus FLoL for both nozzles is also depicted in Figure 19 in two unique ways. The main purpose of the line connecting all identical boundary conditions on the left side is to show how the fuel trend fluctuates depending on the chamber and fuel conditions. The pattern of the change in chamber conditions with a constant fuel is represented on the other side by a line connecting all of the identical fuel types. Monitoring the trend of chamber and fuel adjustments is made much easier by this method. With the data on the right side of Figure 19, it is apparent that the increase in FLoL when ignition is delayed is consistent with the change in chamber temperature. In line with the current observations, correlation 17 also showed a negative correlation between chamber temperature and FLoL.

FLoL and chamber pressure have a correlation that is similar to the ignition delay time pattern (the right side of Figure 19). Due to the lack of OH* formation, lower oxygen concentration causes cooler flame cores, which not only prolongs the FLoL but also delays the prior ignition delay; this pattern is consistent with correlation 17 and other research [73, 74].

Figures 18 and 19 illustrate the inverse relationship between ignition delay and FLoL as fuel pressure differs. The trend suggests that when pressure rises, the FLoL increases and goes against the way the ignition delay behaves. Numerous arguments have been presented in the academic literatures to justify this trend [11, 39, 46, 75]. Pickett et al. [46] emphasized that FLoL is introduced when the spray velocity matches the flame propagation velocity. Consequently, higher injection pressure increases the velocity of fuel droplets, which then drops to the velocity of flame propagation further from the injector

nozzle tip [39], moreover, when injection velocity increases, fuel moves farther from the nozzle tip [11].

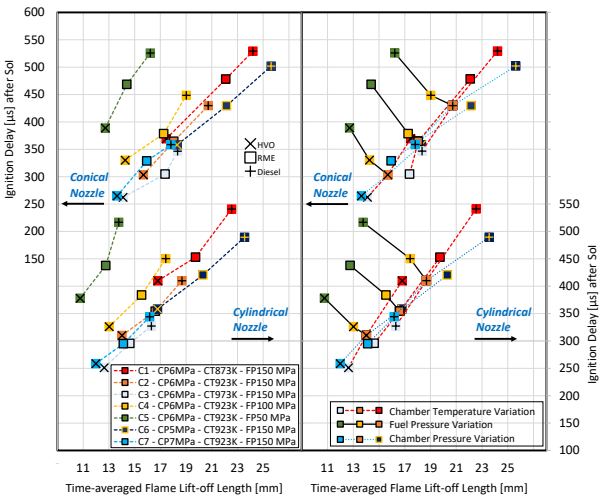

Figure 19. Ignition Delay [µs] after SoI vs. Time-averaged Flame Lift-off Length [mm] – Cylindrical and Conical Nozzles

Similarly, the left side of Figure 19 demonstrates that ignition delay and FLoL have the same correlation for all of the indicated fuels. The FLoL increases in accordance with the lengthening of the ignition delay from the shortest (HVO) to the longest (Diesel). In general, there is not always a consistent link between FLoL and ignition delay for diverse fuel structures. For a variety of specialty fuels, the other authors have similarly noted a variety of variations and levels of uncertainty [46, 76, 77]. As a result, this tendency is not always true, and comparing oxygenated fuels to hydrocarbon fuels or paraffinic fuels to non-paraffinic fuels is challenging.

The cylindrical nozzle has a 10% shorter FLoL, according to the overall tendency when comparing the nozzles. This trend shows the availability of a nearly stoichiometric air-to-fuel ratio across a larger area of the cylindrical nozzle, particularly upstream of the spray, which results in a shorter FLoL. The blue rectangular boxes next to each test result on Figure 18 already show the proportion of shorter FLoL of the cylindrical nozzle. There is no discernible difference in the behaviour of the nozzles between those with short and those with long ignition delay times.

Soot Appearance Time

Soot, the natural flame luminosity, is compared with ignition delay times in this section as it was described in the optical technique section. Figure 20 shows the probability time for soot formation, which was determined using a cumulative Gaussian distribution. The chemical composition of the fuel, the nozzle features, the local air-to-fuel ratio, which is primarily controlled by oxygenated fuel, air temperature and density, and FLoL all have an impact on soot formation.

In general, the spray and combustion processes for diesel-type fuels can be divided into four stages [11, 44, 78-80]:

1- The first stage is meant to take place when the majority of the fuel is still liquid, before the high-temperature reaction. Mie-Scattering, which was more completely discussed in the preceding sections, was used to successfully record this phase.

2- The second stage starts when fuel droplets begin to evaporate and combine with air after absorbing heat from the hot ambient gas. The liquid droplet is sheared and atomized until it is forced to evaporate by the jet velocity and surrounding density. This phase initiates the first air-to-fuel mixing zones around the jet edge and lasts until the initial OH*

signal is detected. As previously mentioned, the rate at which the near-stoichiometric zone forms is greatly influenced by fuel oxygen content, specifications of the fuel, the geometry of the nozzles, the air pressure, and the temperature. The first flame kernels are created during this stage.

3- The reactive spray keeps penetrating and exchanging momentum with the ambient air until it reaches the fraction of ignitable fuel mixture. The main combustion phase, or premixed combustion stage, increases quickly at this point, and the fuel releases its greatest amount of heat. This marks the conclusion of the ignition delay stage. The amount of heat emitted during this phase is significantly influenced by how well the fuel and air were premixed in the preceding step. Flame propagation moves upstream toward reactants at this stage.

4- The mixing-controlled diffusion flame (late combustion phase), which dominates the primary soot formation stage, is controlled by a shorter ignition delay and a faster burning of fuel injected during the preceding stage (prior to auto-ignition). This is the result of locally increased temperature and pressure. The rate of combustion is primarily regulated by the rate of fuel injection. Currently, the flame luminosity is really bright.

In the combustion of fuels similar to diesel, the premixed and diffusion stages are distinguished by the rate of flame heat release. At the start of the premixed phase of combustion, the heat release rises sharply, and then it falls to a moderate level at the start of the diffusion phase. Since the current chamber is constant volume and constant pressure, no pressure increase is observed during the development of combustion, making it impossible to determine the rate of heat release accurately. As a result, it is hard to determine whether soot production marks the start of the diffusion phase or not.

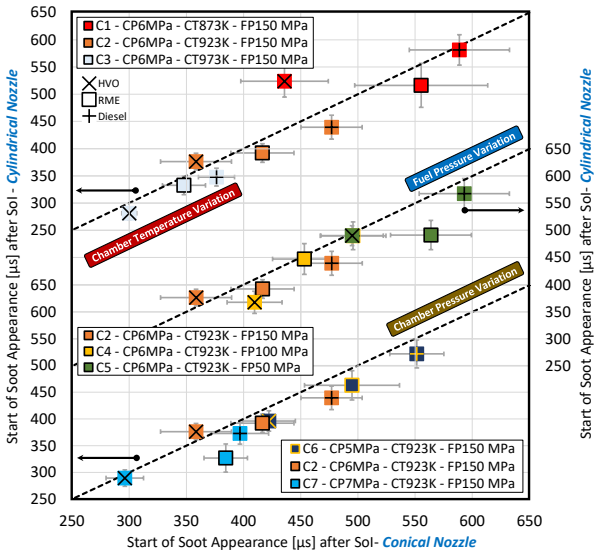

Figure 20. The Time of Soot Appearance Initiation [µs] after SoI – Cylindrical and Conical Nozzles

The data obtained from Figure 20 reveals that most of the points on the first side follow the ignition delay pattern. Soot development is delayed in proportion to the delay in ignition. According to the trend for the first category, a rise in chamber temperature speeds up the start of soot formation, which is consistent with the rule of ignition progression.

Although no soot formation can be detected in the rich mixture at the initial ignition process (due to a delay in soot formation in the premixed phase of combustion), it is generally accepted that initial soot formation begins to produce nearly rich air-to-fuel zones [45, 81]. As a result, Figure 21 is provided as an addition to the data

shown in Figure 20 regarding the interval between the start of the ignition and the development of soot. Figure 21 then shows that chamber temperature also influences the time between ignition and soot production. A shorter duration can be observed since combustion happens at a richer air-to-fuel mixture when ignition is advanced at higher temperatures. Additionally, the FLoL is shorter, which reduces the amount of time it takes for the air to mix with fuel before combustion initiation. These all have a role in a richer combustion taking place at a higher temperature. The formation of soot begins more quickly in a richer area of the spray, which is the main reason for a shorter duration at a higher chamber temperature. Additionally, a faster reaction rate, which causes the shorter premixed phase, impacts this trend.

However, Figure 21 shows that the air pressure and fuel pressure, the other two boundary variations, are similarly inversely proportional to this duration. This time is shortened due to the previously mentioned effects of increased air pressure and fuel pressure.

One factor to bear in mind is that some areas of the cylindrical nozzle do not follow these general rules. It is possible to come to the conclusion that nozzle characteristics, cavitation, and fuels under various conditions all influence this behaviour. Each point is repeated 32 times and the standard deviations of the ignition delay and soot appearance times in these points are roughly the same as other points, especially with HVO fuel. Although the effect of experiment conditions cannot be completely disregarded. When using HVO fuel, Bjørgen et al. [41] noticed a similar pattern in which soot formation is slightly increased as the ignition delay is shortened. For such a situation, they proposed a partially premixed air-to-fuel combination that resulted in a local equivalence ratio that ranged from very lean to very rich.

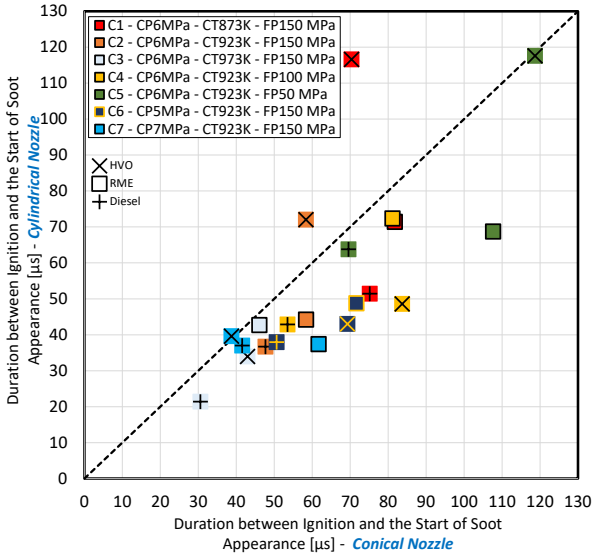

Figure 21. Duration between Ignition and the Start of Soot Appearance [µs] – Cylindrical and Conical Nozzles

On the one hand, soot formation is related to the ignition time, which is more effective; on the other hand, fuel composition is also an influential parameter on the commencement of soot formation. Mueller et al. [82] have demonstrated that hydrocarbon fuels produce more soot than paraffinic fuels due to inclusion of more aromatic compounds. This indicates that soot formation is more likely to begin faster with diesel than with other fuels. RME, on the other hand, has a lower carbon content than diesel, allowing it to produce less soot. Additionally, its higher oxygen content in the flame centerline leads in a lowered and delayed soot level. According to Manin et al. [83], oxygen in fuel not only speeds up soot oxidation and

lowers soot formation, but it also moves the process closer to the nozzle.

The general trend of nozzles comparison in soot formation time and the duration between ignition and soot also prove faster soot formation in the cylindrical nozzle, which is mostly attributable to its shorter FLoL and faster ignition delay.

This section compared the two nozzles mentioned earlier and provided detailed information about combustion initiation and propagation. In general, as chamber temperature, pressure, and fuel pressure increase, the ignition delay time advances. The section has already provided some details on how well boundary conditions affect the initial air-to-fuel stoichiometric region. The cylindrical nozzle demonstrated faster ignition as a result of its ability to produce a faster initial stoichiometric ratio, which was driven by its wider cone angle and greater air entrainment capability. Following this behaviour, it has the capacity to lower the FLoL at all conditions. The boundary conditions, fuel varieties, and nozzle geometries also displayed a general trend between ignition time and FLoL and proved longer FLoL with retarted ignition time, with the exception of fuel pressure. On the other hand, it was illustrated that boundary conditions and nozzle geometries are significantly useful for determining the times for the ignition-to-soot durations since the time of soot formation comes first from the ignition time and is then affected by the circumstances. The explanations about the findings have already been discussed in detail in this section.

Summary:

In a CVC, two background gases were used to monitor the performance of two large diesel injectors. The nitrogen gas was used to analyze the jet and liquid spray phases, while dry air was used to evaluate the combustion characteristics. Seven experimental conditions were tested with three different fuel types (Reference diesel, HVO, and RME) using nozzles of equal exit diameter but different shapes: a conical nozzle (K factors of 4) with twice the length of a cylindrical nozzle (K factors of 0). A summary of the results are as follows:

1- The mixture composition remains constant regardless of the fuel mass flow rate and indicates that both mass balance and enthalpy balance occur at the same axial distance without any discernible effect.

2- The evaluation of all spray parameters have proved that the cone angle is an injector geometry-based parameter.

3- The results demonstrate a 13% larger jet cone angle, a 24% shorter liquid spray penetration, and a 13% lower fuel mass flow rate in the cylindrical nozzle.

4- The cylindrical nozzle entrains substantially more air into the spray plume than the conical nozzle at the initial time of injection, demonstrating its ability to improve mixture formation and advance the initial air-to-fuel stoichiometric region prior to combustion.

The results proved a raise in the air-to-fuel mass ratio by about 28% (at the same penetration lengths).

5- A significant reduction in the igniting delay time was achieved at nearly all sites in the cylindrical nozzle, thanks to faster fuel evaporation and a higher rate of air entrainment. This tendency is greatly affected by a higher cavitation and turbulence levels as well as a wider cone angle. Finally, the cylindrical nozzle showed an average of 4.5% shorter ignition delay time and 10% lower FLoL.

6- Mixture formation in the cylindrical nozzle has a significant impact before ignition, while the ignition time and FLoL have the most effects on the mixture quality during combustion. A shorter FLoL and faster ignition time in the cylindrical nozzle resulted in a richer air-to-fuel mixture and affected soot production.

7- There is a general trend between FLoL and ignition delay time, where delaying ignition results in longer FLoL. However, fuel injection pressure variation exhibits unique and diverse behaviour, explained by fuel droplet velocity and movement farther downstream of the combustion zone.

8- The trend of soot appearance time between the two nozzles follows the ignition delay time pattern. However, the duration between ignition and soot appearance time varies between different test operating points due to the influence of nozzle geometries and boundary conditions on soot formation. The combustion development causes the soot production in the cylindrical nozzle to occur 5.9% more quickly with a variety of ignition-to-soot durations.

References:

[1] M. Blessing, G. König, C. Krüger, U. Michels, V. Schwarz. Analysis of flow and cavitation phenomena in diesel injection nozzles and its effects on spray and mixture formation. SAE transactions. (2003) 1694-706.

[2] S. Riess, T. Klima, M. Wensing, A. Braeuer. Influence of Bio-Diesel and Ethanol on the Diesel Engine Process Chain Investigated by Optical Measurement Techniques. ILASS–Europe Brighton, UK, 2016.

[3] A.H. Farajollahi, R. Firuzi, M. Rostami, F. Bagherpor. Consideration of the effects of increasing spray cone angle and turbulence intensity on heavy-duty diesel engine pollution and specific outputs using CFD. International Journal of Engine Research. 24 (2021) 373-92.

[4] H. Taghavifar, S. Khalilarya, S. Jafarmadar, F. Baghery. 3-D numerical consideration of nozzle structure on combustion and emission characteristics of DI diesel injector. Applied Mathematical Modelling. 40 (2016) 8630-46.

[5] J.-S. Han, P.-H. Lu, X.-B. Xie, M.-C. Lai, N.A. Henein. Investigation of diesel spray primary break-up and development for different nozzle geometries. SAE Transactions. (2002) 2528-48.

[6] J. Benajes, J.V. Pastor, R. Payri, A.H. Plazas. Analysis of the influence of diesel nozzle geometry in the injection rate characteristic. J Fluids Eng. 126 (2004) 63-71.

[7] R. Payri, J. García, F. Salvador, J. Gimeno. Using spray momentum flux measurements to understand the influence of diesel nozzle geometry on spray characteristics. Fuel. 84 (2005) 551-61.

[8] R. Payri, J.P. Viera, V. Gopalakrishnan, P.G. Szymkowicz. The effect of nozzle geometry over internal flow and spray formation for three different fuels. Fuel. 183 (2016) 20-33.

[9] H. Chaves, M. Knapp, A. Kubitzek, F. Obermeier, T. Schneider. Experimental study of cavitation in the nozzle hole of diesel injectors using transparent nozzles. SAE transactions. (1995) 645-57.

[10] F. Payri, V. Bermúdez, R. Payri, F. Salvador. The influence of cavitation on the internal flow and the spray characteristics in diesel injection nozzles. Fuel. 83 (2004) 419-31.

[11] R. Payri, J.P. Viera, V. Gopalakrishnan, P.G. Szymkowicz. The effect of nozzle geometry over ignition delay and flame lift-off of reacting direct-injection sprays for three different fuels. Fuel. 199 (2017) 76-90.

[12] R. Payri, F.J. Salvador, J. Gimeno, J. De la Morena. Effects of nozzle geometry on direct injection diesel engine combustion process. Applied thermal engineering. 29 (2009) 2051-60.

[13] S. Som, A.I. Ramirez, D.E. Longman, S.K. Aggarwal. Effect of nozzle orifice geometry on spray, combustion, and emission characteristics under diesel engine conditions. Fuel. 90 (2011) 1267-76.

[14] A. Peter, S. Riess, M. Wensing, J. Fruehhaber, T. Lauer. Investigation of Mixture Formation and Flammability of Natural Gas and Diesel under Dual Fuel Operating Conditions in the Limits of Flame-quenching and Knocking. The Proceedings of the International symposium on diagnostics and modeling of combustion in internal combustion engines. The Japan Society of Mechanical Engineers2017. p. C302.

[15] S. Riess, L. Weiss, A. Peter, J. Rezaei, M. Wensing. Air entrainment and mixture distribution in Diesel sprays investigated by optical measurement techniques. International Journal of Engine Research. 19 (2018) 120-33.

[16] H. Fajri, R.C. Mallada, S. Riess, L. Strauß, M. Wensing. Mixture Formation Analysis for Diesel, n-Dodecane, RME, and HVO in Large-Scale Injector Nozzles. SAE Technical Paper. (2022).

[17] R.V. Payri, Juan P; Gopalakrishnan, Venkatesh; Szymkowicz, Patrick G. The effect of nozzle geometry over the evaporative spray formation for three different fuels. Fuel. 188 (2017) 645-60.

[18] W. Jing, W.L. Roberts, T. Fang. Spray combustion of Jet-A and diesel fuels in a constant volume combustion chamber. Energy Conversion and Management. 89 (2015) 525-40.

[19] Y. Wakuri, M. Fujii, T. Amitani, R. Tsuneya. Studies on the penetration of fuel spray in a diesel engine. Bulletin of JSME. 3 (1960) 123-30.
[20] J.D. Naber, D.L. Siebers. Effects of gas density and vaporization on penetration and dispersion of diesel sprays. SAE transactions. (1996) 82-111.
[21] D. Siebers, B. Higgins. Flame lift-off on direct-injection diesel sprays under quiescent conditions. SAE Transactions. (2001) 400-21.
[22] D. Siebers, B. Higgins, L. Pickett. Flame lift-off on direct-injection diesel fuel jets: oxygen concentration effects. Sae Transactions. (2002) 1490-509.
[23] Q.S. KHAN, S.W. Baek, H. Ghassemi. On the autoignition and combustion characteristics of kerosene droplets at elevated pressure and temperature. Combustion science and technology. 179 (2007) 2437-51.
[24] A.K. Agarwal. Biofuels (alcohols and biodiesel) applications as fuels for internal combustion engines. Progress in energy and combustion science. 33 (2007) 233-71.
[25] A. Hassaneen, A. Munack, Y. Ruschel, O. Schroeder, J. Krahl. Fuel economy and emission characteristics of Gas-to-Liquid (GTL) and Rapeseed Methyl Ester (RME) as alternative fuels for diesel engines. Fuel. 97 (2012) 125-30.
[26] A. Omari, S. Pischinger, O.P. Bhardwaj, B. Holderbaum, J. Nuottimäki, M. Honkanen. Improving engine efficiency and emission reduction potential of HVO by fuel-specific engine calibration in modern passenger car diesel applications. SAE International Journal of Fuels and Lubricants. 10 (2017) 756-67.
[27] H. Aatola, M. Larmi, T. Sarjovaara, S. Mikkonen. Hydrotreated Vegetable Oil (HVO) as a Renewable Diesel Fuel: Trade-off between NO_x, Particulate Emission, and Fuel Consumption of a Heavy Duty Engine. SAE International Journal of Engines. 1 (2009) 1251-62.
[28] J.J. López, O.A. De la Garza, J. De la Morena, S. Martínez-Martínez. Effects of cavitation in common-rail diesel nozzles on the mixing process. International Journal of Engine Research. 18 (2017) 1017-34.
[29] J.J. López, O.A. de la Garza, J. De la Morena, S. Martínez-Martínez. Influence of Cavitation in Common-Rail Diesel Nozzles on the Soot Formation Process through Measuring Soot Emissions. Energies. 14 (2021) 6267.
[30] A. Tsolakis, A. Megaritis, M. Wyszynski, K. Theinnoi. Engine performance and emissions of a diesel engine operating on diesel-RME (rapeseed methyl ester) blends with EGR (exhaust gas recirculation). Energy. 32 (2007) 2072-80.
[31] D. Qi, H. Chen, L. Geng, Y.Z. Bian. Experimental studies on the combustion characteristics and performance of a direct injection engine fueled with biodiesel/diesel blends. Energy Conversion and Management. 51 (2010) 2985-92.
[32] P. Bielaczyc, A. Szczotka, P. Gizynski, I. Bedyk. The effect of pure RME and biodiesel blends with high RME content on exhaust emissions from a light duty diesel engine. SAE Technical Paper. (2009).
[33] R. Payri, J. Gimeno, G. Bracho, D. Vaquerizo. Study of liquid and vapor phase behavior on Diesel sprays for heavy duty engine nozzles. Applied Thermal Engineering. 107 (2016) 365-78.
[34] R. Balz, I.G. Nagy, G. Weisser, D. Sedarsky. Experimental and numerical investigation of cavitation in marine Diesel injectors. International Journal of Heat and Mass Transfer. 169 (2021) 120933.
[35] R. Balz, G. Bernardasci, B. von Rotz, D. Sedarsky. Influence of nozzle geometry on spray and combustion characteristics related to large two-stroke engine fuel injection systems. Fuel. 294 (2021) 120455.
[36] R. Payri, G. Bracho, P. Marti-Aldaravi, A. Viera. Nozzle Geometry Size Influence on Reactive Spray Development: From Spray B to Heavy Duty Applications. SAE Technical Paper2017.
[37] C.L. Genzale, R.D. Reitz, M.P. Musculus. Effects of spray targeting on mixture development and emissions formation in late-injection low-temperature heavy-duty diesel combustion. Proceedings of the combustion institute. 32 (2009) 2767-74.
[38] J. Rezaei. Fuel Sprays Phase Change at Diesel Engine Ambient Conditions: Phase Equilibrium Non-Ideality. Friedrich-Alexander-Universität Erlangen-Nürnberg (FAU)2021.
[39] J. Pastor, R. Payri, J. Gimeno, J. Nerva. Experimental study on RME blends: Liquid-phase fuel penetration, chemiluminescence, and soot luminosity in diesel-like conditions. Energy & fuels. 23 (2009) 5899-915.
[40] B. Higgins, D. Siebers. Measurement of the flame lift-off location on DI diesel sprays using OH chemiluminescence. SAE Transactions. (2001) 739-53.
[41] K.O.P. Bjørgen, D.R. Emberson, T. Løvås. Combustion and soot characteristics of hydrotreated vegetable oil compression-ignited spray flames. Fuel. 266 (2020) 116942.
[42] J. Kojima, Y. Ikeda, T. Nakajima. Spatially resolved measurement of OH*, CH*, and C2* chemiluminescence in the reaction zone of laminar methane/air premixed flames. Proceedings of the Combustion institute. 28 (2000) 1757-64.
[43] T. Hoffmann, P. Hottenbach, H.-J. Koss, C. Pauls, G. Grünefeld. Investigation of mixture formation in Diesel sprays under quiescent conditions using Raman, Mie and LIF diagnostics. (2008).
[44] Q. Cheng, H. Tuomo, O. Kaario, L. Martti. HVO, RME, and diesel fuel combustion in an optically accessible compression ignition engine. Energy & Fuels. 33 (2019) 2489-501.
[45] M. Jakob, T. Huelser, A. Janssen, P. Adomeit, S. Pischinger, G. Gruenefeld. Simultaneous high-speed visualization of soot luminosity and OH∗ chemiluminescence of alternative-fuel combustion in a HSDI diesel engine under realistic operating conditions. Combustion and Flame. 159 (2012) 2516-29.
[46] L.M. Pickett, D.L. Siebers, C.A. Idicheria. Relationship between ignition processes and the lift-off length of diesel fuel jets. SAE transactions. (2005) 1714-31.
[47] H. Wu, K. Nithyanandan, B. Li, T.H. Lee, C.-f.F. Lee, C. Zhang. Investigation on spray and soot lift-off length of an ABE-diesel blend in a constant volume chamber with diesel engine conditions. Internal Combustion Engine Division Fall Technical Conference. American Society of Mechanical Engineers2014. p. V001T02A11.
[48] S. Rieß. Einfluss von Kraftstoff und Abgasrückführung auf Gemischbildung und Verbrennung von dieselmotorischen Sprays. Shaker Verlag2017.
[49] A. Peter. Charakterisierung der Gemischbildung und Zündung in konventionellen Diesel- und Dual-Fuel-Brennverfahren. Shaker Verlag2022.
[50] S. Riess, L. Weiss, J. Rezaei, A. Peter, M. Wensing. The liquid penetration of diesel substitutes. Ilass Europe 28th european conference on Liquid Atomization and Spray Systems. Editorial Universitat Politècnica de València2017. pp. 1060-113.
[51] B. Wang, Y. Li, Y. Jiang, H. Xu, X. Zhang. Dynamic spray development of 2-methylfuran compared to ethanol and isooctane under ultra-high injection pressure. Fuel. 234 (2018) 581-91.
[52] A. Montanaro, L. Allocca, M. Lazzaro. Iso-octane spray from a GDI multi-hole injector under non-and flash boiling conditions. SAE Technical Paper2017.
[53] H. Versteeg, G. Hargrave, B. Myatt, D. Lewis, T. Church, G. Brambilla. Using phase Doppler anemometry & high speed imaging to analyze MDI spray plume dynamics. (2017).
[54] Petroleum products — Determination of the ignition quality of diesel fuels — Cetane engine method. (ISO Standard No. 5165:2017), 2017. p. 20.
[55] Flüssige Mineralölerzeugnisse - Bestimmung der indizierten Cetanzahl (ICZ) von Kraftstoffen aus Mitteldestillaten - Verfahren mittels Kalibrierung mit primären Bezugskraftstoffen unter Verwendung einer Verbrennungskammer mit konstantem Volumen; Deutsche Fassung. (DIN EN 17155:2018), 2018. p. 29.
[56] G. Lequien, S. Skeen, J. Manin, L.M. Pickett, O. Andersson. Ignition quality effects on lift-off stabilization of synthetic fuels. SAE International Journal of Engines. 8 (2015) 625-34.
[57] P. Simacek, I. Soucek, M. Pospisil, D. Vrtiska, H. Kittel. Impact of hydrotreated vegetable oil and biodiesel on properties in blends with mineral diesel fuel. Thermal Science. 23 (2019) 1769-77.
[58] M. Parravicini, C. Barro, K. Boulouchos. Experimental characterization of GTL, HVO, and OME based alternative fuels for diesel engines. Fuel. 292 (2021).
[59] O.P. Bhardwaj, A.F. Kolbeck, T. Kkoerfer, M. Honkanen. Potential of hydrogenated vegetable oil (HVO) in future high efficiency combustion system. SAE International Journal of Fuels and Lubricants. 6 (2013) 157-69.
[60] C. Bachler, S. Schober, M. Mittelbach. Simulated distillation for biofuel analysis. Energy & fuels. 24 (2010) 2086-90.
[61] J. Desantes, F. Salvador, J.J. López, J. De la Morena. Study of mass and momentum transfer in diesel sprays based on X-ray mass distribution measurements and on a theoretical derivation. Experiments in fluids. 50 (2011) 233-46.
[62] S. Som, D.E. Longman, A.I. Ramirez, S. Aggarwal. Influence of nozzle orifice geometry and fuel properties on flow and cavitation characteristics of a diesel injector. Fuel injection in automotive engineering. (2012) 112-26.
[63] F. Brusiani, S. Falfari, P. Pelloni. Influence of the Diesel injector hole geometry on the flow conditions emerging from the nozzle. Energy Procedia. 45 (2014) 749-58.
[64] L.M. Pickett, D.L. Siebers. Orifice diameter effects on diesel fuel jet flame structure. J Eng Gas Turbines Power. 127 (2005) 187-96.

[65] Z.-Y. Sun, G.-X. Li, C. Chen, Y.-S. Yu, G.-X. Gao. Numerical investigation on effects of nozzle's geometric parameters on the flow and the cavitation characteristics within injector's nozzle for a high-pressure common-rail DI diesel engine. Energy Conversion and Management. 89 (2015) 843-61.
[66] S. Rieß, Durst, A., Wensing, M., & Wang, J. . An advanced optical metrology view on mixture formation in Diesel sprays. In Proceedings of the 13th International AVL Symposium on Propulsion Diagnostics, Baden-Baden, 2018.
[67] A. Peter, T. Klima, S. Riess, L. Weiss, A. Braeuer, M. Wensing. Quantitative mixture formation analysis of diesel sprays. 14th Triennial Int Conf on Liquid Atomization and Spray Systems, ICLASS2018. pp. 22-6.
[68] P. Lakshminarayanan, Y.V. Aghav. Ignition delay in a diesel engine. Modelling diesel combustion. Springer2010. pp. 59-78.
[69] J.-J. Whang, C.-Y. Yukao, J.-T. Ho, S.-C. Wong. Experimental study of the ignition of single droplets under forced convection. Combustion and flame. 110 (1997) 366-76.
[70] R. Stauch, S. Lipp, U. Maas. Detailed numerical simulations of the autoignition of single n-heptane droplets in air. Combustion and flame. 145 (2006) 533-42.
[71] G. Lequien, Z. Li, O. Andersson, M. Richter. Lift-off length in an optical heavy-duty diesel engine. SAE International Journal of Engines. 8 (2015) 635-46.
[72] N. Zhou, M. Huo, H. Wu, K. Nithyanandan, F.L. Chia-fon, Q. Wang. Low temperature spray combustion of acetone–butanol–ethanol (ABE) and diesel blends. Applied Energy. 117 (2014) 104-15.
[73] K.D. Cung, A.A. Moiz, X. Zhu, S.-Y. Lee. Ignition Process and Flame Lift-Off Characteristics of dimethyl ether (DME) Reacting Spray. Frontiers in Mechanical Engineering. 7 (2021) 547204.
[74] F. Payri, J.V. Pastor, J.-G. Nerva, J.M. Garcia-Oliver. Lift-off Length and KL extinction measurements of biodiesel and Fischer-Tropsch fuels under quasi-steady diesel engine conditions. SAE International Journal of Engines. 4 (2011) 2278-97.
[75] K. Nishida, J. Zhu, X. Leng, Z. He. Effects of micro-hole nozzle and ultra-high injection pressure on air entrainment, liquid penetration, flame lift-off and soot formation of diesel spray flame. International Journal of Engine Research. 18 (2017) 51-65.
[76] S. Kook, L.M. Pickett. Soot volume fraction and morphology of conventional, fischer-tropsch, coal-derived, and surrogate fuel at diesel conditions. SAE International Journal of Fuels and Lubricants. 5 (2012) 647-64.
[77] L.M. Pickett, D.L. Siebers. Fuel effects on soot processes of fuel jets at DI diesel conditions. SAE transactions. (2003) 2044-66.
[78] C. Satyanarayana, P. Rao. Influence of key properties of pongamia biodiesel on performance combustion and emission characteristics of a DI diesel engine. Wseas transaction on heat and Mass Transfer. 4 (2009) 34-44.
[79] S. Narayan. Noise and vibration characteristics of a micro car diesel engine. University of Roma Tre2016.
[80] T. Kamimoto, H. Kobayashi. Combustion processes in diesel engines. Progress in Energy and Combustion Science. 17 (1991) 163-89.
[81] J.E. Dec. A conceptual model of DL diesel combustion based on laser-sheet imaging. SAE Technical Paper. 106 (1997) 1319-48.
[82] C.J. Mueller, W.J. Pitz, L.M. Pickett, G.C. Martin, D.L. Siebers, C.K. Westbrook. Effects of oxygenates on soot processes in DI diesel engines: experiments and numerical simulations. SAE transactions. (2003) 964-82.
[83] J. Manin, S. Skeen, L. Pickett, E. Kurtz, J.E. Anderson. Effects of oxygenated fuels on combustion and soot formation/oxidation processes. SAE International Journal of Fuels and Lubricants. 7 (2014) 704-17.

Acknowledgement:

This project has received funding from the European Union Horizon 2020 Research and Innovation programme. Grant Agreement No. 861002.

Definitions, Acronyms, Abbreviations

a	calibration constant
A_o	nozzle exit area
b	constant
c	constant
C_a	area contraction coefficient
C_d	discharge coefficient
C_v	velocity contraction coefficient
d	constant
d_o	nozzle exit diameter
d_i	nozzle entrance diameter
e	constant
f	constant
f_{st}	stoichiometric air-to-fuel ratio
g	constant
K	geometric shape of nozzle
$\dot{m}_a$	entrained air mass flow rate
$\dot{m}_f$	fuel mass flow rate
P_a	chamber pressure
P_f	fuel pressure
S	total jet penetration
T_a	chamber temperature
u_f	fuel velocity
u_o	initial fuel velocity
Z_{st}	chamber oxygen concentration
Δm	total mass of injected fuel
Δt	injection duration
μ	expected value of Gaussian distribution
σ	standard deviation of Gaussian distribution
ρ_a	chamber density
ρ_f	fuel density
θ	jet cone angle

CVC Chamber	Constant Volume Combustion
FLoL	Flame Lift-off Length
fps	Frame per Second
HBW	Half Bandwidth
HVO	Hydrotreated Vegetable Oils
OH-PLIF	OH-Planar Laser Induced Fluorescence
PAH-PLIF	Polycyclic Aromatic Hydrocarbons-Planar Laser Induced Fluorescence
RME	Rapeseed Methyl Ester
SoI	Start of Injection